Adaptive Rate NOMA for Cellular IoT Networks

G. Sreya, S. Saigadha, Praful D. Mankar, Goutam Das, Harpreet S. Dhillon

Abstract—Internet-of-Things (IoT) technology is envisioned to enable a variety of real-time applications by interconnecting billions of sensors/devices. These IoT devices rely on low-power wide-area wireless connectivity for transmitting, mostly fixed- but small-size, status updates of the random processes observed by them. Owing to their ubiquity, cellular networks are seen as a natural candidate for providing reliable wireless connectivity to IoT devices. Given the massive number of IoT devices, enabling non-orthogonal multiple access (NOMA) for the mobile users and IoT devices is appealing in terms of the efficient utilization of spectrum compared to the orthogonal multiple access (OMA). For instance, the uplink NOMA can also be configured such that the mobile users adapt their transmission rates depending upon the channel conditions while the IoT devices transmit at a fixed rate. For this setting, we analyze the ergodic capacity of the mobile users and the mean local delay of IoT devices using stochastic geometry. Our analysis demonstrates that the aforementioned NOMA configuration provides better ergodic capacity for mobile users compared to OMA when delay constraint of IoT devices is strict. We also show that NOMA supports a larger packet size at IoT devices than OMA under the same delay constraint.

Index Terms—Adaptive rate NOMA, cellular networks, ergodic rate, IoT networks, mean local delay, stochastic geometry.

I. Introduction

The IoT networks provide a digital fabric interconnecting billions of wireless devices for exchanging application-specific information without any human intervention. Many IoT applications, such as smart cities and traffic surveillance, rely on the real-time processing of information received from a massive number of sensors/devices deployed over a large area. The key research challenges for realizing such IoT applications are to facilitate flexible deployment, wide-area coverage, low power devices, and low device complexity. The cellular networks are seen as a natural candidate for providing wide coverage to IoT devices on a massive scale [1]. However, the low-cost IoT devices may not be capable of performing complex signal processing needed for the advanced antenna array communication techniques (such as millimeter communication). Besides, the IoT devices may experience much higher pathloss if they are deployed in places like tunnels or basements or are simply located far away from the BSs. Thus, efficient link budget planning is also crucial for low-power IoT devices. For these reasons, the sub-6 GHz band is primarily being considered to support low power wide area (LPWA) links of the low-cost IoT devices [2]. However, the sub-6 GHz band is crowded with the existing mobile services. This motivates spectral resource sharing between IoT devices and mobile users [3].

G. Sreya, S. Saigadha and G. Das are with IIT Kharagpur, India (Email: {sreya.gopakumar, saigadha000}@gmail.com and gdas@gssst.iitkgp.ac.in). P. D. Mankar is with SPCRC, IIIT Hyderabad, India (Email: praful.mankar@iiit.ac.in). H. S. Dhillon is with Wireless@VT, Department of ECE, Virginia Tech, Blacksburg, VA 24061, USA (Email: hdhillon@vt.edu). The work of H. S. Dhillon was supported by the U.S. National Science Foundation under Grants CPS-1739642 and CNS-1814477.

Further, the IoT devices are generally deployed to share observations/measurements of some physical process in the form of fixed and small payloads at random intervals. As a result, the BSs require to support small size data packet transmissions from a massive number of low-power IoT devices [4], [5]. In release 13, 3GPP LTE included enhanced machine type communications (eMTC) and narrowband IoT (NB-IoT) communication to offer narrowband LPWA links to IoT devices in the sub-6 GHz band [6], [7]. On the other hand, non-orthogonal multiple access (NOMA) can be used as a viable alternative to improve spectral utilization as well as enable massive access in IoT networks [8]. In the literature, the design of NOMA-based IoT networks is extensively investigated. For instance, [9] presents NOMA-aided NB-IoT networks for enhanced connectivity, [10] presents ALOHA-based NOMA scheme for scalable and energy-efficient deployment of IoT networks, and [11] studies the performance of NOMA-based wireless powered IoT networks. However, most existing works on the design of NOMA-aided IoT networks are investigated in simplified settings, such as a single-cell system.

Recently, stochastic geometry has emerged as a powerful tool for modeling and analyzing a variety of large-scale wireless networks. However, works on the analysis of NOMA-aided IoT networks using stochastic geometry are relatively sparse, a few of which are briefly discussed below. The authors of [12] analyze aggregators-assisted two-hop NOMA-enabled cellular IoT network by modeling the locations of IoT devices, aggregators and BSs as independent Poisson point processes (PPPs). Therein, aggregators are employed to relay the NOMA transmissions from the IoT devices to the BS. The authors of [13] analyze RF energy harvesting based cellular IoT networks under the PPP setting. The IoT devices first harvest energy using downlink signals and then perform the uplink data transmission using NOMA. While the existing works in this direction consider pairing of IoT devices for non-orthogonal access, NOMA can also offer an efficient solution to the co-existence of mobile users and IoT devices by pairing their transmissions in the same spectral resource, as considered in this paper. The authors of [14] analyze the throughput performance of NOMA-based uplink transmission of mobile users and IoT devices in cellular networks under the PPP setting. However, the authors apply random pairing (i.e., mobile user and IoT device are randomly selected for a cell), which undermines the NOMA performance gains.

The authors of [15] show that it is imperative to pair devices with distinctive link qualities for harnessing maximum performance gains from fixed-power NOMA. The authors of [16] characterized the performance gain of NOMA over OMA, termed the *large-scale near-far gain*, which is a result of the variation in link distances of NOMA users. Inspired by this, we consider a new pairing scheme that selects a mobile user

from the *Johnson Mehl (JM) cells* [17] to ensure the mobile user with shorter link distance (i.e., good channel quality) is selected for pairing, as will be discussed shortly. In most cases, this approach will ensure distinctive link qualities of the mobile user and IoT device selected for pairing.

Contributions: This paper presents a new stochastic geometry-based analysis of uplink NOMA for the non-orthogonal transmission of mobile users and IoT devices in cellular networks with power control. In particular, we consider adaptive rate NOMA wherein the mobile users adapt modulation and coding scheme (MCS) according to the time-varying channel and the IoT devices transmit fixed but small-size data packets. We assume that the locations of IoT devices, mobile users and BSs follow independent PPPs. Further, we consider mobile users with serving link distance below threshold L for pairing to ensure the distinct link quality criteria for harnessing the optimum NOMA performance gain [15]. As a result, the mobile user and IoT device are selected for pairing from the *Johnson Mehl (JM) cell* [17] and *Poisson Voronoi (PV) cell*, respectively, corresponding to their associated BS.[1] For this setup, we first derive the moments of the *meta distribution* [18] for both mobile users and IoT devices. Next, we use these results to characterize the achievable ergodic capacity for the typical mobile user and the mean local delay observed by the typical IoT device. Finally, our numerical results validate the analytical findings and demonstrate that adaptive rate NOMA is more spectrally-efficient than OMA when the delay constraint of IoT devices is strict.

II. SYSTEM MODEL

We assume that the locations of BSs, mobile users and IoT devices form independent homogeneous PPPs Φ'_{b}, Φ_{m} and Φ_{t} of densities λ_{b}, λ_{m} and λ_{t}, respectively, on $\mathbb{R}^2$. We present the uplink analysis for the typical BS placed the origin o by adding an additional point at o to Φ'_{b}. Let $\Phi_{\mathrm{b}} = \Phi'_{\mathrm{b}} \cup \{o\}$. For more details on this typical cell viewpoint, please refer to [19]. Mobile users and IoT devices are assumed to associate with their nearest BSs. Thus, the mobile users and IoT devices associated with BS at $\mathbf{x}$ must lie within *Poisson Voronoi (PV) cell* which is $V_{\mathbf{x}} = \{\mathbf{y} \in \mathbb{R}^2 : \|\mathbf{x} - \mathbf{y}\| \leq \|\mathbf{z} - \mathbf{y}\|, \mathbf{z} \in \Phi_{\mathrm{b}}\}$.

It is important to pair devices with distinct link qualities to achieve NOMA benefits [15]. Therefore, we pair mobile users with serving link distances shorter than L with the IoT devices. This ensures that the mobile users experiencing good channel quality are involved in the NOMA pairing. Thus, the NOMA pair associated with a BS at $\mathbf{x}$ includes the mobile user within the JM cell $\mathcal{V}_{\mathbf{x}} = \mathcal{B}_{\mathbf{x}}(L) \cap V_{\mathbf{x}}$ [17] and the IoT device within the PV cell $V_{\mathbf{x}}$, where $\mathcal{B}_{\mathbf{x}}(L)$ is a ball of radius L centered at $\mathbf{x}$. Note that L controls the fraction of mobile users available for pairing. This fraction is equal to $\mathcal{A}_{\mathrm{L}} = 1 - \exp(-\pi\lambda_{\mathrm{b}}L^2)$ [20], which clearly increases with L.

In the proposed uplink NOMA, we consider that the BS first decodes the mobile users' signal in the presence of intra-cell interference from its paired IoT device. Next, the BS applies

successive interference cancellation (SIC) technique to remove the intra-cell interference to the IoT device from the mobile user. After that, it decodes the IoT devices' signal. Thus, we effectively consider multi-user detection by SIC.

We assume that each mobile user has perfect knowledge of its uplink signal to interference ratio (SIR) and can employ infinitely many MCS levels such that there is an MCS level that achieves Shannon capacity with an arbitrarily small BER for a realized SIR. Under this SIR adaptive MCS selection, the transmission rate of the mobile user is $\log_2(1 + \beta_{\mathrm{m}})$ when the realized SIR is β_{m}. This is also beneficial to improve the rate of successful transmission for the IoT devices as the BS will always be able to successfully perform the SIC operation because of the mobile user's channel adaptive transmission strategy. We term this scheme the *adaptive rate NOMA*. The IoT devices are assumed to transmit at a fixed rate as they may not be complex enough to transmit with adaptive MCS.

This paper assumes that each BS employs NOMA transmission of IoT devices and mobile users (from JM cells) over the same spectral band and uses different spectral band for the transmission of mobile users lying outside of the JM cells. We assume the standard power law path-loss model with exponent α, and consider that both mobile users and IoT devices transmit using a distance-proportional fractional power control scheme. We use subscript $i \in \{\mathrm{m}, \mathrm{t}\}$ for denoting the mobile user (i.e., $i = \mathrm{m}$) and the IoT device (i.e., $i = \mathrm{t}$). Thus, the transmit power of device i is $\rho_i R_i^{\alpha(\epsilon_i)}$ where R_i, ρ_i and $\epsilon_i \in [0, 1]$ denote its serving link distance, baseline transmit power and power control fraction, respectively. Let Ψ_{t} and Ψ_{m} denote the point processes of the inter-cell interfering IoT devices and mobile users, respectively. Let $R_{\mathbf{x}_i}$ and $D_{\mathbf{x}_i}$ denote the distances of device i located at $\mathbf{x}$ from its serving BS and the typical BS placed at o. We assume independent Rayleigh fading over all links. The received SIR at the typical BS at o from the mobile user in $\mathcal{V}_o$ is

$$\mathrm{SIR}_{\mathrm{m}} = \frac{\rho_{\mathrm{m}} h_{\mathrm{m}} R_{\mathrm{m}}^{\alpha(\epsilon_{\mathrm{m}}-1)}}{\rho_{\mathrm{t}} h_{\mathrm{t}} R_{\mathrm{t}}^{\alpha(\epsilon_{\mathrm{t}}-1)} + I_{\mathrm{m}} + I_{\mathrm{t}}}, \tag{1}$$

and the SIR received at the typical BS at o from the IoT device in V_o after removing the intra-cell interference via SIC is

$$\mathrm{SIR}_{\mathrm{t}} = \frac{\rho_{\mathrm{t}} h_{\mathrm{t}} R_{\mathrm{t}}^{\alpha(\epsilon_{\mathrm{t}}-1)}}{I_{\mathrm{m}} + I_{\mathrm{t}}}, \quad \text{where} \tag{2}$$

$I_{\mathrm{m}} = \sum_{\mathbf{x} \in \Psi_{\mathrm{m}}} \rho_{\mathrm{m}} h_{\mathbf{x}_{\mathrm{m}}} R_{\mathbf{x}_{\mathrm{m}}}^{\alpha\epsilon_{\mathrm{m}}} D_{\mathbf{x}_{\mathrm{m}}}^{-\alpha}$ and $I_{\mathrm{t}} = \sum_{\mathbf{x} \in \Psi_{\mathrm{t}}} \rho_{\mathrm{t}} h_{\mathbf{x}_{\mathrm{t}}} R_{\mathbf{x}_{\mathrm{t}}}^{\alpha\epsilon_{\mathrm{t}}} D_{\mathbf{x}_{\mathrm{t}}}^{-\alpha}$,

where $h_i \sim \exp(1)$ and $h_{\mathbf{x}_i} \sim \exp(1)$ are the small scale fading gains of intended device and interfering device at $\mathbf{x}$, respectively, for $i \in \{\mathrm{m}, \mathrm{t}\}$.

The conditional success probability (conditioned on the locations of the mobile user $\mathbf{y}_{\mathrm{m}}$, IoT device $\mathbf{y}_{\mathrm{t}}$ and the inter-cell interferers' point process $\Psi = \Psi_{\mathrm{m}} \cup \Psi_{\mathrm{t}}$) for the mobile user and the IoT device with SIR thresholds β_{m} and β_{t} are

$$\mathrm{P}_{\mathrm{m}}(\beta_{\mathrm{m}}; \mathbf{y}, \Psi) = \mathbb{P}(\mathrm{SIR}_{\mathrm{m}} > \beta_{\mathrm{m}} | \mathbf{y}, \Psi), \text{ and} \tag{3}$$

$$\mathrm{P}_{\mathrm{t}}(\beta_{\mathrm{m}}, \beta_{\mathrm{t}}; \mathbf{y}, \Psi) = \mathbb{P}(\mathrm{SIR}_{\mathrm{m}} > \beta_{\mathrm{m}}, \mathrm{SIR}_{\mathrm{t}} > \beta_{\mathrm{t}} | \mathbf{y}, \Psi), \tag{4}$$

where $\mathbf{y} = \mathbf{y}_{\mathrm{m}} \cup \mathbf{y}_{\mathrm{t}}$. The success probability of the IoT

---

[1]This paper considers only a subset of the mobile users (from JM cells) for NOMA pairing, and the remaining mobile users (outside of JM cells) are assumed to be served in a conventional manner. The analysis for users outside the JM cell can be followed from [18] with small improvisations.

device depends on the joint decoding of messages of both the devices. However, because of the assumption of the adaptive transmission, the mobile user's signal is always decodable at the BS with arbitrarily small error probability. Hence, its intra-cell interference to the IoT devices can be eliminated using SIC because of which (4) reduces to

$$P_t(\beta_t; \mathbf{y}, \Psi) = \mathbb{P}(SIR_t > \beta_t | \mathbf{y}, \Psi). \tag{5}$$

The distribution of conditional success probability, termed *meta distribution* [18], is useful in studying the network performance in terms of the percentage of devices experiencing success probability above some pre-defined threshold. Hence, we aim to derive the meta distributions for both the mobile user and IoT device under the aforementioned NOMA strategy.

Under the adaptive transmission strategy, the *ergodic rate* of the typical mobile user is

$$\mathcal{R}_m = \mathbb{E}[\log_2(1 + SIR_m)]. \tag{6}$$

As the IoT devices are deployed to transmit their observations in a timely manner, it is meaningful to characterize their performance using the *mean local delay*. The mean local delay is defined in [18] as the mean number of transmissions needed for the successful delivery of a packet.

III. ANALYSIS OF ADAPTIVE RATE NOMA

The link distance distribution and the point processes of the inter-cell interfering devices are crucial for the meta distribution analysis, which we will discuss next. Recall, we assume that the paired mobile user and IoT device are located uniformly at random within $\mathcal{V}_o$ and V_o, respectively. The probability density function (pdf) of the link distance R_t of IoT device can be approximated as

$$f_{R_t}(r) = 2\pi\rho\lambda_b r \exp(-\pi\rho\lambda_b r^2), \quad r \geq 0, \tag{7}$$

where $\rho = 9/7$ [20]. The serving link distance R_m of the mobile user is bounded by L as it is selected from $\mathcal{V}_o$. Hence, its pdf can be obtained by truncating (7) as

$$f_{R_m}(r) = \frac{2\pi\rho\lambda_b r \exp\left(-\pi\rho\lambda_b r^2\right)}{1 - \exp\left(-\pi\rho\lambda_b L^2\right)}, \quad 0 \leq r \leq L. \tag{8}$$

Now, we characterize the inter-cell interferers' point processes Ψ_m and Ψ_t in the following. Both these processes are non-stationary since the inter-cell interfering devices lie outside V_o. It is well-known that the exact characterization of uplink interferers' point process is difficult. However, an accurate approximation of the pair correlation function (pcf) of Ψ_m as seen from the typical BS is derived in [17] as $g_m(r) = 1 - \exp(-2\pi\bar{\mathcal{V}}_o^{-1}r^2)$, where $\bar{\mathcal{V}}_o^{-1} = \mathbb{E}[|\mathcal{V}_o|^{-1}]$ and $|A|$ denotes the area of set A. Using this pcf and the fact that there is a single interfering user from each cell, we can approximate Ψ_m using a non-homogeneous PPP with density

$$\tilde{\lambda}_m(r) = \lambda_b g_m(r). \tag{9}$$

The pcf of Ψ_t can be obtained simply by replacing $\bar{\mathcal{V}}_o^{-1}$ with $\mathbb{E}[|V_o|^{-1}] \approx \frac{7}{5}\lambda_b$ (which corresponds to the case $L \to \infty$) as $g_t(r) = 1 - \exp(-\frac{14}{5}\pi\lambda_b r^2)$, which exactly matches with the pcf derived in [21]. Thus, similar to Ψ_m, we can also

approximate Ψ_t using a non-homogeneous PPP with density

$$\tilde{\lambda}_t(r) = \lambda_b g_t(r). \tag{10}$$

Now, in the following, we analyze the meta distributions of SIR_m and SIR_t. It is well-known that the exact expression for meta distribution is difficult to derive. Hence, similar to [18], we focus on deriving the moments of these meta distributions.

Theorem 1. *The b-th moment of meta-distribution of the typical mobile user under the adaptive rate NOMA is*

$$M_b^m = \mathbb{E}_{R_m}[\mathcal{I}_1(s_m)\mathcal{I}_2(s_m)\mathcal{M}(s_m)], \tag{11}$$

where $s_m = \frac{\beta_m}{\rho_m} R_m^{\alpha(1-\epsilon_m)}$,

$$\mathcal{I}_1(s_m) = \mathbb{E}_{R_t}\left[\left(1 + s_m\rho_t R_t^{\alpha(\epsilon_t-1)}\right)^{-b}\right],$$

$$\mathcal{I}_2(s_m) = \exp\left(-2\pi\int_0^\infty \tilde{\lambda}_t(u)\left(1 - \int_0^u (1+\right.\right.$$
$$\left.\left. s_m\rho_t r^{\alpha\epsilon_t}u^{-\alpha})^{-b}f_{R_{\mathbf{x}_t}}(r|u)\mathrm{d}r\right)u\mathrm{d}u\right),$$

$$\mathcal{M}(s_m) = \exp\left(-2\pi\int_0^\infty \tilde{\lambda}_m(u)\left(1 - \int_0^{\min(u,L)}(1+\right.\right.$$
$$\left.\left. s_m\rho_m r^{\alpha\epsilon_m}u^{-\alpha})^{-b}f_{R_{\mathbf{x}_m}}(r|u)\mathrm{d}r\right)u\mathrm{d}u\right),$$

and pdf*s of* R_t, R_m, $R_{\mathbf{x}_t}$ *and* $R_{\mathbf{x}_m}$ *are given in* (7), (8), (22) *and* (21).

Proof. Please refer to the Appendix for the proof. □

Corollary 1. *The b-th moment of meta-distribution of the typical mobile user under OMA is*

$$\tilde{M}_b^m = \mathbb{E}_{R_m}[\mathcal{M}(s_m)], \tag{12}$$

where s_m *and* $\mathcal{M}(s_m)$ *are given in Theorem 1.*

Now, we present moments of meta distributions for the IoT device under the adaptive rate NOMA and OMA strategies.

Theorem 2. *The b-th moment of meta-distribution of the typical IoT device under the adaptive rate NOMA is*

$$M_b^t = \mathbb{E}_{R_t}[\mathcal{I}_2(s_t)\mathcal{M}(s_t)], \tag{13}$$

where $s_t = \frac{\beta_t}{\rho_t} R_t^{\alpha(1-\epsilon_t)}$, $\mathcal{I}_2(s_t)$ *and* $\mathcal{M}(s_t)$ *are given in* (11).

Proof. From (5), the conditional coverage probability of the typical IoT device located at $\mathbf{y}_t$ is

$$P_t(\beta_t; \mathbf{y}, \Psi) = \mathbb{P}\left(h_t > I_m s_t + I_t s_t | \mathbf{y}, \Psi\right),$$
$$\overset{(a)}{=} \prod_{\mathbf{x}\in\Psi_m}\frac{1}{1 + s_t\rho_m R_{\mathbf{x}_m}^{\alpha\epsilon_m} D_{\mathbf{x}_m}^{-\alpha}}\prod_{\mathbf{x}\in\Psi_t}\frac{1}{1 + s_t\rho_t R_{\mathbf{x}_t}^{\alpha\epsilon_t} D_{\mathbf{x}_t}^{-\alpha}},$$

where (a) follows from the assumption that $h_t, h_{\mathbf{x}_m}$ and $h_{\mathbf{x}_t} \sim \exp(1)$ and since Ψ_m and Ψ_t are independent.

Now, b-th moment of meta distribution can be obtained as $M_b^t = \mathbb{E}[P_t^b(\beta_t; \mathbf{y}, \Psi)]$. Further, following the similar steps given in the proof of Theorem 1, we obtain (13). □

Corollary 2. *The b-th moment of meta-distribution of the typical IoT device under OMA is given by*

$$\tilde{M}_b^t = \mathbb{E}_{R_t}[\mathcal{I}_2(s_t)], \tag{14}$$

where s_t and $\mathcal{I}_2(s_t)$ are given in Theorem 2.

The first moment of the conditional success probability is the spatially averaged distribution of SIR. Thus, the complementary CDFs of SIR_m under NOMA and OMA becomes

$$\bar{F}_m(\beta_m) = M_1^m \quad \text{and} \quad \tilde{F}_m(\beta_m) = \tilde{M}_1^m, \tag{15}$$

respectively. In OMA, each BS is considered to schedule its associated mobile users and IoT devices for η and $1 - \eta$ fractions of time. Using (15), we now present the ergodic rate of the typical mobile user in the following theorem.

Corollary 3. *Ergodic rates of the typical mobile user under NOMA and OMA, respectively, are*

$$\mathcal{R}_m = \frac{1}{\ln(2)} \int_0^\infty \frac{1}{1 + \gamma} \bar{F}_m(\gamma) \mathrm{d}\gamma, \tag{16}$$

$$\text{and } \tilde{\mathcal{R}}_m = \frac{\eta}{\ln(2)} \int_0^\infty \frac{1}{1 + \gamma} \tilde{F}_m(\gamma) \mathrm{d}\gamma. \tag{17}$$

Corollary 4. *Mean local delay of the typical IoT device under NOMA and OMA, respectively, are*

$$\mathrm{D}_t(\beta_t) = M_{-1}^t \text{ and } \tilde{\mathrm{D}}_t(\beta_t) = (1 - \eta)^{-1} \tilde{M}_{-1}^t. \tag{18}$$

The optimal selection of power control fractions ϵ_m and ϵ_t is crucial to maximize the ergodic rate for the mobile user. However, maximizing the ergodic rate of the mobile user may negatively impact the mean local delay for the IoT device. Therefore, we consider maximizing the ergodic rate of the mobile user under the constraint of maximum mean local delay of the IoT device for NOMA and OMA cases as below

$$\mathcal{P}_{\text{NOMA}} : \max_{(\epsilon_m, \epsilon_t)} \mathcal{R}_m, \quad \text{s.t } \mathrm{D}_t(\beta_t) \leq \tau, \tag{19}$$

$$\mathcal{P}_{\text{OMA}} : \max_{(\eta, \epsilon_m, \epsilon_t)} \tilde{\mathcal{R}}_m, \quad \text{s.t. } \tilde{\mathrm{D}}_t(\beta_t) \leq \tau, \tag{20}$$

where τ represents a predefined threshold. Under the fixed-rate NOMA, the successful transmission of IoT device is conditioned on the successful decoding of the mobile device's signal. Thus, the fixed-rate NOMA will lead to an inferior mean local delay performance for the IoT device compared to the adaptive rate NOMA. As a result, the IoT device requires smaller transmission power (and thus smaller intra-cell interference to the mobile user) to ensure the mean local delay is below threshold τ under the adaptive rate NOMA compared to the fixed-rate NOMA. Therefore, the adaptive rate NOMA provides higher ergodic rate compared to the throughput achievable under the fixed rate NOMA.

IV. NUMERICAL RESULTS AND DISCUSSIONS

We consider $\lambda_b = 10^{-4}$, $\mathcal{A}_L = 0.25$, $\alpha = 4$, $\beta_t = -5$ dB and $\rho_m = \rho_t = 1$, unless mentioned otherwise. Fig. 1 (left) verifies the accuracy of the first moment of meta distribution derived for the mobile users and IoT devices under the adaptive rate NOMA for different values of (ϵ_m, ϵ_t). The first moments of meta distribution of mobile users decreases and IoT devices increases with the increase in ϵ_t for a given ϵ_m.

We compare the proposed NOMA with the conventional OMA in terms of the rate distribution and optimal ergodic rate of mobile users in Fig. 1 (middle) and the mean local delay of IoT devices in Fig. 1 (right). Fig. 1 (middle) presents the rate distribution and ergodic rate for optimally configured NOMA and OMA. It is not surprising to see that the NOMA provides improved rate distribution compared of OMA for $\tau = 2$ (i.e., a strict delay constraint). This is because in OMA, the IoT device requires higher medium access probability (i.e., $1 - \eta$) to ensure its delay constraint when τ is small which allows smaller transmission times for mobile user. Whereas NOMA allows continuous medium access to mobile users with some interference from IoT devices. Besides, the figure shows that NOMA underperforms for $\tau = 10$ (i.e., a loose delay constraint). This is because under OMA, the IoT device require smaller $1 - \eta$ to ensure delay constraint for higher τ and thus it allows the mobile user to transmit more often.

Fig. 1 (right) shows the mean local delay for the IoT device with full power control. It can be observed that the delay is better under NOMA compared to OMA. Besides, it is not sensitive to ϵ_m since SIC is always successful for the adaptive NOMA. However, the delay performance under OMA is very sensitive to η, which is expected. The figure also shows that the mean local delay degrades with the increase of SIR threshold β_t and also with the increase of ϵ_m under NOMA and η under OMA. It also demonstrates that for a given threshold τ, NOMA can be configured such that it meets the delay constraint with a larger β_t compared to that under OMA case. This implies that NOMA can support a larger message size as compared to OMA under the same delay constraint. Besides, it also shows that the mean delay does not significantly change for a wide range of ϵ_m under the NOMA whereas it drastically degrades with a moderate increase in η under OMA.

Furthermore, it is expected that the ergodic rate under both NOMA and OMA degrades with the increase of L. This is because a larger JM cell accommodates more mobile users with lower SIR_ms. The optimal fraction $\mathcal{A}_L$ of mobile users involved in the non-orthogonal transmission with IoT devices depends on the network design parameters, such as bandwidth partitioning for NOMA and non-NOMA users, scheduling policy, and load distributions of mobile and IoT services. This investigation is a promising direction for future research.

V. CONCLUSION

We proposed an adaptive rate NOMA scheme for enabling massive access in cellular-supported IoT applications wherein an IoT device and a mobile user are paired for non-orthogonal transmission. The proposed *adaptive rate NOMA* assumes that the mobile users adapt their MCS according to the channel conditions whereas IoT devices transmit small size packets using fixed MCS. Using stochastic geometry, we characterized the moments of the meta distribution for both types of devices, which are then used to characterize the ergodic rate for the typical mobile user and the mean local delay for the typical IoT device. Our results demonstrated that the adaptive rate NOMA provides better transmission rates for the mobile users as compared to the OMA under strict mean local delay constraint of IoT devices. This suggests that the proposed NOMA scheme is a spectrally-efficient solution for meeting capacity and delay requirements of mobile users and IoT devices, respectively.
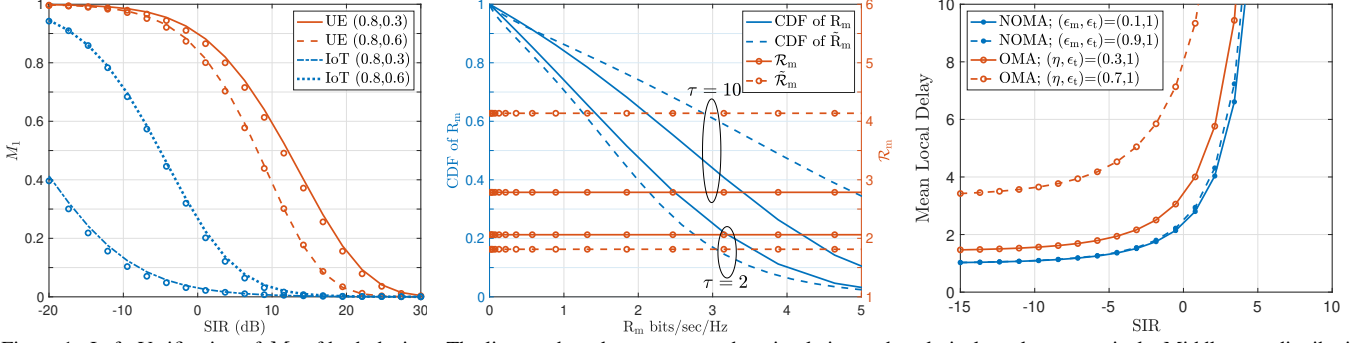
Figure 1. Left: Verification of M_1 of both devices. The lines and markers correspond to simulation and analytical results, respectively. Middle: rate distribution and ergodic rate for optimally configured NOMA and OMA. Right: mean local delay of IoT devices for various power control fractions ($\epsilon_\mathrm{m}, \epsilon_\mathrm{t}$).

APPENDIX

Letting $s_\mathrm{m} = \beta_\mathrm{m}\rho_\mathrm{m}^{-1}R_\mathrm{m}^{\alpha(1-\epsilon_\mathrm{m})}$, the conditional success probability of the mobile user located at $\mathbf{y}_\mathrm{m}$ can be obtained as

$$\mathrm{P}_\mathrm{m}(\beta_\mathrm{m}; \mathbf{y}, \Psi) = \mathbb{P}\left(h_\mathrm{m} > s_\mathrm{m}\left(\rho_\mathrm{t}h_\mathrm{t}R_\mathrm{t}^{\alpha(\epsilon_\mathrm{t}-1)} + I_\mathrm{m} + I_\mathrm{t}\right)|\mathbf{y}, \Psi\right)$$

$$\overset{(a)}{=} \prod_{\mathbf{x}\in\Psi_\mathrm{m}} \frac{1 + s_\mathrm{m}\rho_\mathrm{t}R_\mathrm{t}^{\alpha(\epsilon_\mathrm{t}-1)}}{1 + s_\mathrm{m}\rho_\mathrm{m}R_{\mathbf{x}_\mathrm{m}}^{\alpha\epsilon_\mathrm{m}}D_{\mathbf{x}_\mathrm{m}}^{-\alpha}} \prod_{\mathbf{x}\in\Psi_\mathrm{t}} \frac{1}{1 + s_\mathrm{m}\rho_\mathrm{t}R_{\mathbf{x}_\mathrm{t}}^{\alpha\epsilon_\mathrm{t}}D_{\mathbf{x}_\mathrm{t}}^{-\alpha}},$$

where (a) follows since $h_\mathrm{m}, h_\mathrm{t}, h_{\mathbf{x}_\mathrm{m}}$ and $h_{\mathbf{x}_\mathrm{t}} \sim \exp(1)$. Since $R_{\mathbf{x}_\mathrm{m}} \leq D_{\mathbf{x}_\mathrm{m}}$, for $\mathbf{x} \in \Psi_\mathrm{m}$, pdf of $R_{\mathbf{x}_\mathrm{m}}$ can be truncated as

$$f_{R_{\mathbf{x}_\mathrm{m}}}(r|D_{\mathbf{x}_\mathrm{m}}) = \frac{2\pi\rho\lambda_\mathrm{b}r\exp\left(-\pi\rho\lambda_\mathrm{b}r^2\right)}{1 - \exp(-\pi\rho\lambda_\mathrm{b}\min(L, D_{\mathbf{x}_\mathrm{m}})^2)}. \quad (21)$$

Besides, $R_{\mathbf{x}_\mathrm{t}} \leq D_{\mathbf{x}_\mathrm{t}}$. Thus, the pdf of $R_{\mathbf{x}_\mathrm{t}}$ becomes

$$f_{R_{\mathbf{x}_\mathrm{t}}}(r|D_{\mathbf{x}_\mathrm{t}}) = \frac{2\pi\rho\lambda_\mathrm{b}r\exp(-\pi\rho\lambda_\mathrm{b}r^2)}{1 - \exp(-\pi\rho\lambda_\mathrm{b}D_{\mathbf{x}_\mathrm{t}}^2)}, 0 \leq r \leq D_{\mathbf{x}_\mathrm{t}}. \quad (22)$$

The b-th moment of $\mathrm{P}_\mathrm{m}(\beta_\mathrm{m}; \mathbf{y}, \Psi)$ can be obtained as

$$M_b^\mathrm{m} = \mathbb{E}_{R_\mathrm{m}}\left[\mathbb{E}_{R_\mathrm{t}}\left[\left(1 + s_\mathrm{m}\rho_\mathrm{t}R_\mathrm{t}^{\alpha(\epsilon_\mathrm{t}-1)}\right)^{-b}\right]\right.$$

$$\mathbb{E}_{\Psi_\mathrm{m}, R_{\mathbf{x}_\mathrm{m}}}\left[\prod_{\mathbf{x}\in\Psi_\mathrm{m}}\frac{1}{(1 + s_\mathrm{m}\rho_\mathrm{m}R_{\mathbf{x}_\mathrm{m}}^{\alpha\epsilon_\mathrm{m}}D_{\mathbf{x}_\mathrm{m}}^{-\alpha})^b}\right]$$

$$\left.\mathbb{E}_{\Psi_\mathrm{t}, R_{\mathbf{x}_\mathrm{t}}}\left[\prod_{\mathbf{x}\in\Psi_\mathrm{t}}\frac{1}{(1 + s_\mathrm{m}\rho_\mathrm{t}R_{\mathbf{x}_\mathrm{t}}^{\alpha\epsilon_\mathrm{t}}D_{\mathbf{x}_\mathrm{t}}^{-\alpha})^b}\right]\right]$$

$$= \mathbb{E}_{R_\mathrm{m}}\left[\mathbb{E}_{R_\mathrm{t}}\left[\left(1 + s_\mathrm{m}\rho_\mathrm{t}R_\mathrm{t}^{\alpha(\epsilon_\mathrm{t}-1)}\right)^{-b}\right]\right.$$

$$\mathbb{E}_{\Psi_\mathrm{m}}\left[\prod_{\mathbf{x}\in\Psi_\mathrm{m}}\int_0^{\min(D_{\mathbf{x}_\mathrm{m}}, L)}\frac{1}{(1+\rho_\mathrm{m}s_\mathrm{m}r^{\alpha\epsilon_\mathrm{m}}D_{\mathbf{x}_\mathrm{m}}^{-\alpha})^b}f_{R_{\mathbf{x}_\mathrm{m}}}(r|D_{\mathbf{x}_\mathrm{m}})\mathrm{d}r\right]$$

$$\left.\mathbb{E}_{\Psi_\mathrm{t}}\left[\prod_{\mathbf{x}\in\Psi_\mathrm{t}}\int_0^{D_{\mathbf{x}_\mathrm{t}}}\frac{1}{(1+\rho_\mathrm{t}s_\mathrm{m}r^{\alpha\epsilon_\mathrm{t}}D_{\mathbf{x}_\mathrm{t}}^{-\alpha})^b}f_{R_{\mathbf{x}_\mathrm{t}}}(r|D_{\mathbf{x}_\mathrm{t}})\mathrm{d}r\right]\right].$$

Next, using conditional pdfs of $R_{\mathbf{x}_\mathrm{m}}$ and $R_{\mathbf{x}_\mathrm{t}}$ (given in (21) and (22)), and the probability generating functional of approximate non-homogeneous PPPs Ψ_m and Ψ_t with densities $\tilde{\lambda}_\mathrm{m}(r)$ and $\tilde{\lambda}_\mathrm{t}(r)$ (given in (9) and (10)), we get (11).

REFERENCES

[1] H. S. Dhillon, H. Huang, and H. Viswanathan, "Wide-area wireless communication challenges for the Internet of things," *IEEE Commun. Mag.*, vol. 55, no. 2, pp. 168–174, 2017.

[2] R. Ratasuk, B. Vejlgaard, N. Mangalvedhe, and A. Ghosh, "NB-IoT system for M2M communication," in *IEEE WCNC*, 2016, pp. 1–5.

[3] K. Zheng, F. Hu, W. Wang, W. Xiang, and M. Dohler, "Radio resource allocation in LTE-advanced cellular networks with M2M communications," *IEEE Commun. Mag.*, vol. 50, no. 7, pp. 184–192, 2012.

[4] H. S. Dhillon, H. Huang, H. Viswanathan, and R. A. Valenzuela, "Fundamentals of throughput maximization with random arrivals for m2m communications," *IEEE Trans. Commun.*, vol. 62, no. 11, pp. 4094–4109, 2014.

[5] H. S. Dhillon, H. C. Huang, H. Viswanathan, and R. A. Valenzuela, "Power-efficient system design for cellular-based machine-to-machine communications," *IEEE Trans. Wireless Commun.*, vol. 12, no. 11, pp. 5740–5753, 2013.

[6] R. Ratasuk, B. Vejlgaard, N. Mangalvedhe, and A. Ghosh, "NB-IoT system for M2M communication," in *IEEE WCNC*, 2016, pp. 428–432.

[7] Y.-P. E. Wang, X. Lin, A. Adhikary, A. Grovlen, Y. Sui, Y. Blankenship, J. Bergman, and H. S. Razaghi, "A primer on 3gpp narrowband Internet of things," *IEEE Commun. Mag.*, vol. 55, no. 3, pp. 117–123, 2017.

[8] Z. Ding, X. Lei, G. K. Karagiannidis, R. Schober, J. Yuan, and V. K. Bhargava, "A survey on non-orthogonal multiple access for 5G networks: Research challenges and future trends," *IEEE Journal on Selected Areas in Communications*, vol. 35, no. 10, pp. 2181–2195, 2017.

[9] A. Shahini and N. Ansari, "NOMA aided narrowband IoT for machine type communications with user clustering," *IEEE Internet Things J.*, vol. 6, no. 4, pp. 7183–7191, 2019.

[10] E. Balevi, F. T. A. Rabee, and R. D. Gitlin, "ALOHA-NOMA for massive M2M IoT communication," in *IEEE ICC*, 2018, pp. 1–5.

[11] Q. Wu, W. Chen, D. W. K. Ng, and R. Schober, "Spectral and energy-efficient wireless powered IoT networks: NOMA or TDMA?" *IEEE Trans. Veh. Technol.*, vol. 67, no. 7, pp. 6663–6667, 2018.

[12] H. G. Moussa and W. Zhuang, "Energy- and delay-aware two-hop noma-enabled massive cellular iot communications," *IEEE Internet Things J.*, vol. 7, no. 1, pp. 558–569, 2020.

[13] Z. Ni, Z. Chen, Q. Zhang, and C. Zhou, "Analysis of RF energy harvesting in uplink-NOMA IoT-based network," in *IEEE VTC-Fall*, 2019, pp. 1–5.

[14] M. Kamel, W. Hamouda, and A. Youssef, "Uplink performance of NOMA-based combined HTC and MTC in ultradense networks," *IEEE Internet Things J.*, vol. 7, no. 8, pp. 7319–7333, 2020.

[15] Z. Ding, P. Fan, and H. V. Poor, "Impact of user pairing on 5G nonorthogonal multiple-access downlink transmissions," *IEEE Trans. Veh. Technol.*, vol. 65, no. 8, pp. 6010–6023, 2016.

[16] Z. Wei, L. Yang, D. W. K. Ng, J. Yuan, and L. Hanzo, "On the performance gain of NOMA over OMA in uplink communication systems," *IEEE Trans. Commun.*, vol. 68, no. 1, pp. 536–568, 2020.

[17] P. Parida and H. S. Dhillon, "Stochastic geometry-based uplink analysis of massive MIMO systems with fractional pilot reuse," *IEEE Trans. Wireless Commun.*, vol. 18, no. 3, pp. 1651–1668, 2019.

[18] M. Haenggi, "The meta distribution of the SIR in Poisson bipolar and cellular networks," *IEEE Trans. Wireless Commun.*, vol. 15, no. 4, pp. 2577–2589, 2015.

[19] P. D. Mankar, P. Parida, H. S. Dhillon, and M. Haenggi, "Downlink analysis for the typical cell in poisson cellular networks," *IEEE Wireless Commun. Lett.*, vol. 9, no. 3, pp. 336–339, 2020.

[20] ——, "Distance from the nucleus to a uniformly random point in the 0-cell and the typical cell of the Poisson–Voronoi tessellation," *Journal of Statistical Physics*, vol. 181, no. 5, pp. 1678–1698, 2020.

[21] M. Haenggi, "User point processes in cellular networks," *IEEE Wireless Commun. Lett.*, vol. 6, no. 2, pp. 258–261, 2017.